Compact Toroid Formation using an Annular Helicon Preionization Source

Robert A. Stubbers,[*] Brian E. Jurczyk,[†] Joshua L. Rovey,[‡] Matthew D. Coventry,[§] Darren A. Alman[**]
Starfire Industries LLC, Champaign, IL. 61820

and

Mitchell L.R. Walker[††]
Georgia Institute of Technology, Atlanta, GA. 30332

Formation and ejection of compact plasma toroids for high-thrust and high-specific impulse applications are modeled in conjunction with experimental efforts for concept development. In particular, use of field-reversed configuration plasma with an annular helicon pre-ionization source is being investigated. This type of thruster would have high thrust and no need for electrodes or grids that limit lifetime and reliability. Results from modeling the pulsed power system, the FRC formation process, and acceleration indicate that the annular helicon pre-ionization source is ideal for FRC processes to maximize coupling between the pulsed field and the plasma.

Nomenclature

A	=	area
B	=	magnetic flux density
I	=	current
L	=	characteristic length of the plasma
n	=	number of turns
r	=	radius
t	=	time
V	=	voltage
τ_B	=	magnetic diffusion time
μ	=	permeability of free space
σ	=	plasma conductivity
ϕ	=	magnetic flux

I. Introduction

THE ability of satellites to rapidly perform space maneuvers, between various orbital inclinations, or between geostationary and low earth orbits, is a very desirable capability. These types of maneuvers may be performed by the propulsion system of a separate Orbital Transfer Vehicle (OTV), allowing the satellite to save its reaction mass for station-keeping and nominal on-orbit lifetime. OTV platforms based on chemical propulsion, such as SUMO/FREND, are feasible, but economically questionable due to the short mission lifetime resulting from poor specific impulse. Instead, a high efficiency (> 70%) propulsion system capable of high thrust levels (1 N – 1 kN) with a specific impulse that is at least 5000 s is desirable for commercial viability. Further, electrode-less, scalable, high-power-density systems are desired for lifetime and reliability.

[*] Vice President, Starfire Industries LLC, 60 Hazelwood Drive, Suite 143/203A, AIAA Member.
[†] President, AIAA Member.
[‡] Propulsion Research Engineer, AIAA Member.
[§] Research Engineer.
[**] Research Engineer, AIAA Member.
[††] Assistant Professor, Department of Aerospace Engineering, Guggenheim, AIAA Member.

A promising approach to this problem is a compact-toroid plasma accelerator using an annular helicon ionization source. This new electric thruster has three main processes or stages: 1) ionization/plasma creation using an annular helicon; 2) compact toroidal-plasma creation; and 3) compact toroidal-plasma acceleration. Thrust is generated by the annular helicon with compact toroidal-plasma acceleration (AHCT-PA) thruster through pulsed expulsion of plasma in the form of compact toroids (CTs). Some of the advantages of this type of system are variable thrust for high mission flexibility, electrodeless to mitigate life-limiting erosion processes, gridless to eliminate space-charge voltage limitations, and detached fields to prevent plasma backflow to the spacecraft. Furthermore, it may also have the long-term potential for power generation through fusion processes.[1,2] To determine the feasibility of this thruster concept with an annular helicon preionization source, Starfire Industries and the Georgia Institute of Technology have conducted both numerical and experimental investigations of all three of the thruster mechanisms. The following sections in this paper describe numerical and experimental results studying the creation and acceleration of CTs (process 2 and 3). For information regarding the annular helicon ionization stage (process 1), the reader is referred to Ref. 3.

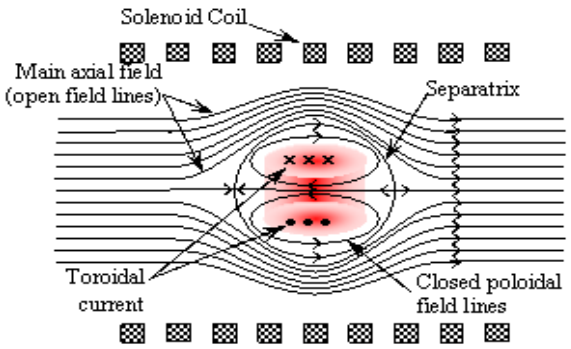

Figure 1: Schematic of a field-reversed configuration plasma noting the induced toroidal current reversal.[4]

The goal of this numerical and experimental investigation is twofold: 1) determine the advantages of an annular geometry for CT formation and acceleration; and 2) experimentally gain experience with pulsed plasma circuitry, diagnostics, and CT formation and acceleration techniques. This is accomplished using the commercially available OOPIC plasma simulation software to model CT creation and acceleration, and by fabricating and testing a pulsed theta coil experiment. Section II describes CTs and traditional formation mechanisms, section III describes the numerical simulations, section IV describes the experimental results, and section V contains the conclusions.

II. Compact Toroids

Compact toroids refer to either a field-reversed configuration (FRC) plasma or a spheromak. In both configurations, an induced plasma current loop produces a magnetic self-field that opposes an externally-applied magnetic field. The FRC is confined by closed poloidal magnetic fields and has zero toroidal field everywhere, whereas the spheromak has an internal toroidal field that vanishes at the wall boundary. Both of these configurations are ideal for space propulsion because external coils are not linked to the plasma and the plasma is on a magnetic island (i.e. completely detached from the spacecraft) such that magnetized plasma does not return to the spacecraft. Figure 1 shows a schematic of an FRC.[4] The combination of the strong toroidal current with an externally applied solenoid field sets up a closed, poloidal magnetic structure inside the solenoid. Because the magnetic lines are closed within the solenoid, particles trapped within will have high confinement time and magnetic detachment from surrounding coils.

Another significant feature of the CT is that the plasma can be translated from a source region along the applied solenoidal field while maintaining its closed configuration, even when ejected at super-Alfvenic speed from the source.[5] A traveling magnetic wave has been used in the past to accomplish this axial acceleration.[6] The force is the result of a gradient in the magnetic field strength across the length of the FRC. Thus, the CT has the following advantages as a propulsion device:

- Self-field magnetic structure and plasma separatrix (self-contained plasma donut without electrode interaction)
- Wall stabilization and low cross-field diffusion coefficients (impressive wall confinement, stability vs. transients, and low particle loss)
- Linear solenoid configuration ejects plasma (allows efficient linear translation and acceleration)

In fusion plasma research, CTs are created by high-current pulse compression such that the plasma is non-adiabatically heated and large densities and temperatures are created (e.g. ion temperature T_i = 50-1000 eV, electron temperature T_e = 50-250 eV, and average density n = 10^{15} cm^{-3}).[7] For space propulsion, low-temperature field

reversal is desired since energy deposited into random thermal motion would need to be extracted by expansion in a magnetic nozzle (which can be done with the compact toroid but is otherwise not necessary). Also, high temperatures would lead to high ionization states and additional line radiation power losses.

The following description of conventional CT formation follows the sequence given by Goldenbaum[8] and Bellan[9] and has four main steps: 1) preionization; 2) implosion; 3) reconnection; and 4) equilibrium. The sequence starts with a gas-filled tube and a straight bias magnetic field generated by a slow external coil. Plasma is then created by a variety of mechanisms, such as a capacitor bank discharged between two electrodes, an RF plasma source, or a DC discharge. This effectively pre-ionizes the gas as shown in Figure 2.[8,9]

Next, a fast capacitor bank discharges through the theta coil and creates a reversed magnetic field. The field is reversed on a time-scale that is less than the magnetic diffusion time ("Implosion" in Figure 2). This fast rising implosion field causes radial compression of the initial bias field. The field lines at the ends of the device reconnect such that the inner bias field becomes the inner poloidal field and the outer implosion field becomes the outer poloidal field. The compressed inner poloidal field necessitates the formation of a toroidal plasma current. At the equilibrium state the CT is composed of a toroidal plasma current with a poloidal magnetic field and is immersed in the outer poloidal field. It is a magnetically detached compact torus (a.k.a.; a CT, compact toroidal-plasma, or plasmoid).

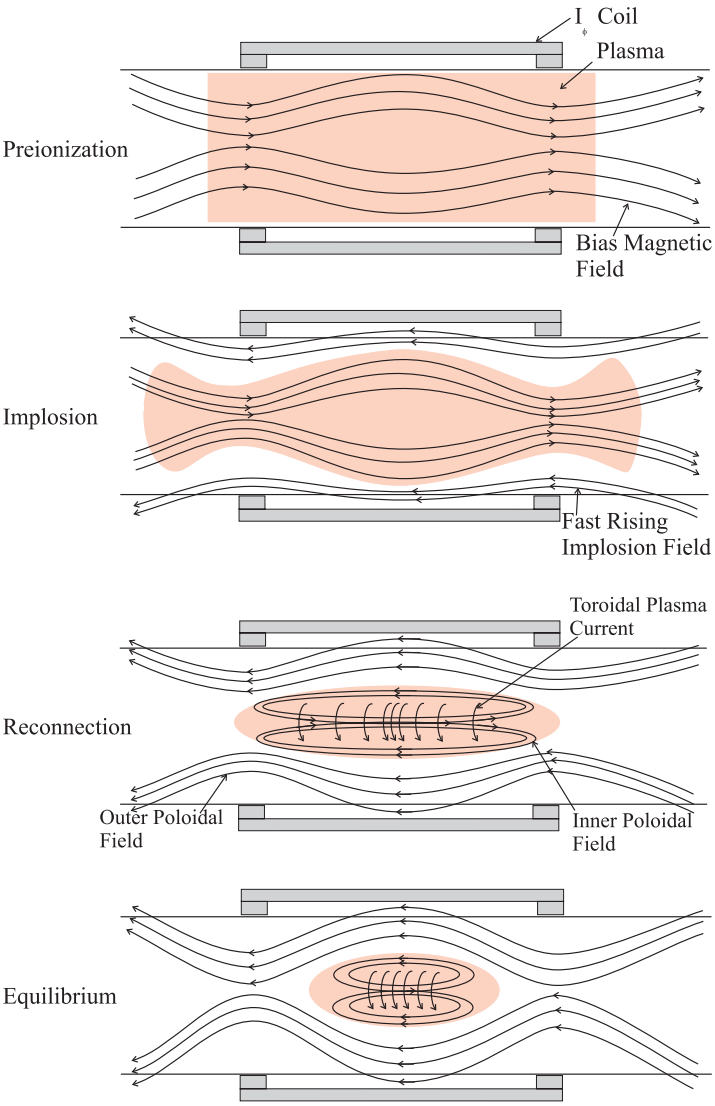

Figure 2: Schematics illustrating the FRC formation process.

III. Numerical Simulations

Preliminary modeling of a cylindrical theta pinch coil with an externally applied bias field demonstrates that an annular target plasma is superior to a conventional helicon due to improved coupling efficiency. The modeling was carried out with hydrogen gas using OOPIC Pro, a commercially available 2D3v particle-in-cell plasma simulation tool. For these simple, illustrative cases, a 17.2-cm-diameter, 20-cm-long pulse coil surrounding a 17-cm-diameter insulating tube was modeled with a bias field of 100 Gauss.

A. Conventional Helicon Geometry

For the conventional helicon-target case, the model geometry, along with the assumed initial plasma density, is shown in Figure 3. Although the particle distribution may appear less dense near the center, it is volumetrically uniform (except near the outer radial edges where the density does decrease). The less-dense appearance is because the particle distribution shown is an aerial projection on to the r-z plane. The centrally peaked density is characteristic of conventional helicon discharges.

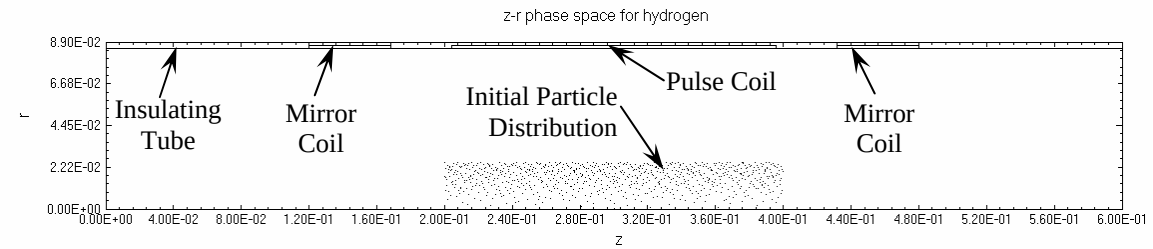

Figure 3: Physical and plasma geometry model for conventional helicon target plasma.

The helicon discharge plasma is simulated by a 5-cm-diameter central high density region (10^{18}/m^3) surrounded by lower density regions (10^{17}/m^3 and 10^{16}/m^3) with a radial thickness of 0.5 cm each. A profile of the initial density distribution is shown in Figure 4. The neutral pressure was 10 mTorr. The pulse current waveform is a sine wave with a frequency of 1 MHz (250 ns to peak) and a peak current of 100 kA in the main coil and 50 kA in each mirror coil. While this rise time is faster than expected from a simple pulse forming network, it reduced computation time while still capturing the physics of FRC formation. Furthermore, it allowed identification of relative performance differences between different preionization techniques. Also, a fast rise time is preferred for increasing coupling of pulse energy into plasma energy. In general, an increase in rate of current rise (dI/dt) leads to better coupling between the pulse and the plasma, which then leads to higher thruster efficiency.

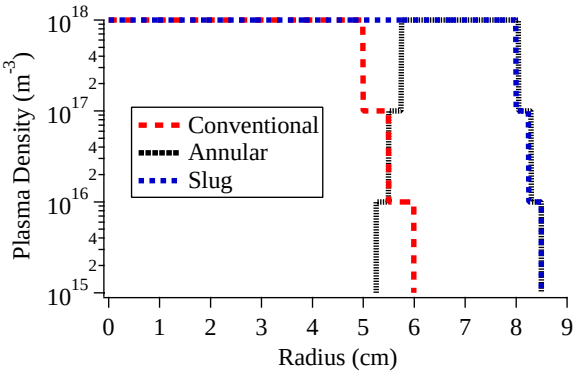

Figure 5: Initial plasma density profiles for the three simulated cases.

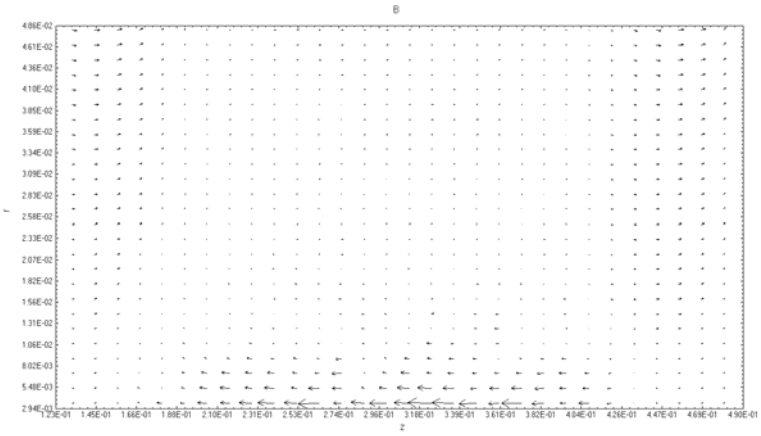

Figure 4: Magnetic field vector in r-z plane showing a small FRC resulting from the conventional helicon model.

Improved coupling with current rise time is related to the plasma skin depth, which scales inversely with the square root of the frequency-conductivity product. To form an FRC, the changing magnetic field created by the pulse coil must create reaction currents in the plasma which prevent the pulsed field from penetrating into the magnetized target plasma. This process is dependent on the plasma having a sufficiently thin skin depth, such that only a thin layer of the plasma is penetrated by (connected to) the pulsed magnetic field. If the plasma skin depth is approximately equal to the radius of the plasma, then an FRC may not form. If the skin depth is a substantial fraction of the plasma radius, much of the plasma will be attached to the open field lines and lost to the walls as the FRC translates into lower field regions. The current in the FRC itself is generated by the bias field trapped in the plasma as it is compressed along with the plasma.

Figure 5 shows a close-up view of the magnetic field vectors (in the r-z plane) of the FRC resulting from the conventional helicon simulation. The FRC has a small diameter, low density, and little trapped flux. The small size is a consequence of the low cross sectional area encompassed by the centrally peaked area. The trapped plasma density and flux are low because the initial plasma volume and flux in the plasma (B-field times cross sectional area) are low.

Because the total plasma density and trapped flux were low, the lifetime of the FRC was short compared to the annular helicon preionization source discussed in the following section. This makes acceleration difficult because the acceleration force applied to the plasma is proportional to the trapped flux. Although the difficulty in

acceleration may be compensated by a low total mass, a higher repetition rate would be required to achieve high thrust. In general, results indicate that a conventional helicon plasma with a plasma density peak on-axis does not seem well-suited for compact toroid formation.

B. Annular Helicon Geometry

The annular helicon discharge plasma was simulated using an annular initial plasma density distribution, as shown in Figure 6. The assumed annular density distribution is composed of low, medium, and high density regions with plasma densities of $10^{16}/m^3$, $10^{17}/m^3$, and, $10^{18}/m^3$, respectively. The high density region had a diameter range of 11.5-16.1 cm, and the surrounding lower density regions were each with an additional diametric thickness of 0.5 cm (0.25 cm inside and 0.25 cm outside). A profile of the initial density distribution is shown in Figure 4. The neutral pressure was 10 mTorr. The pulse current waveform is the same as that used for the conventional helicon simulation discussed previously.

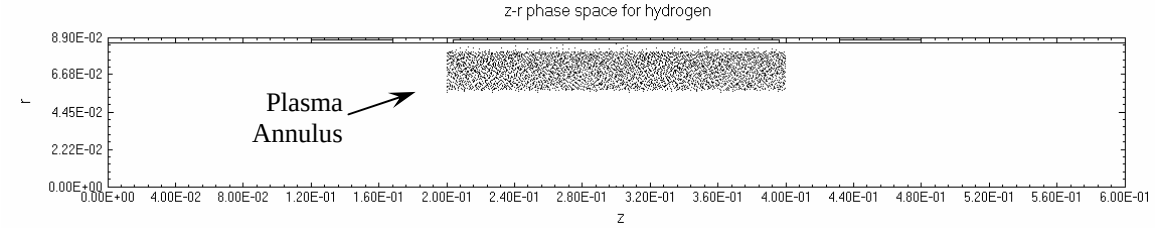

Figure 6: Physical and plasma geometry model for annular helicon target plasma.

Figure 7 shows a close-up view of the resulting magnetic field vector distribution of the formed FRC. An FRC is clearly indicated by the field reversal (arrows pointing left) on axis relative to the pulse field surrounding it (arrows pointing right). Although difficult to see, the magnetic field lines on the ends of the FRC have reconnected within the discharge tube and the FRC plasma is magnetically detached. Compared to the conventional (center-peaked) helicon preionization source, the resulting FRC has larger diameter, trapped flux and mass.

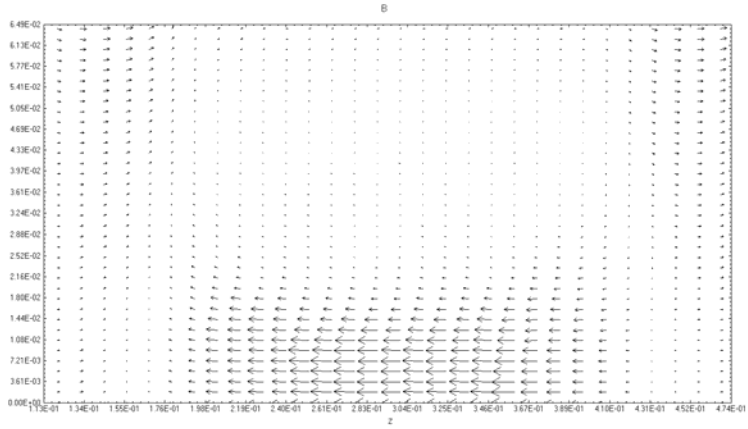

Figure 7: Magnetic field vector in r-z plane of the annular helicon target model showing FRC formation.

C. Uniform Slug Geometry

The annular helicon case was also compared to a slug preionization model, as shown in Figure 8. A profile of the initial density distribution is shown in Figure 4.

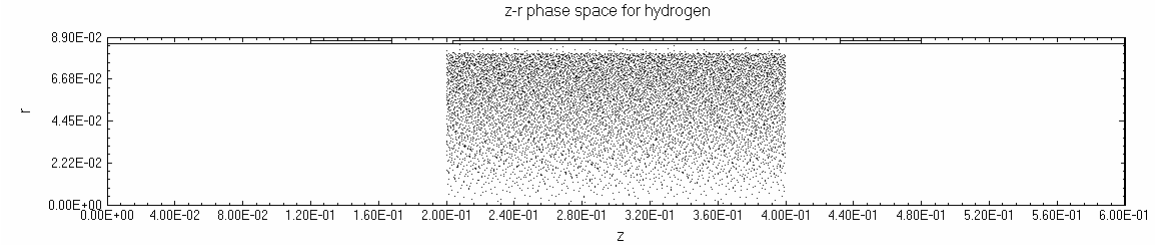

Figure 8: Physical and plasma geometry model for slug target plasma.

Surprisingly, the slug model did not result in FRC formation. The reason that an FRC could not form was because the magnetic field lines could not reconnect at the ends of the would-be FRC. As the current pulse increased, compression of the bias field within the plasma did cause plasma current to increase and a reversed field was formed along the centerline, as shown in Figure 9. However, as the plasma was compressed, it also expanded axially into

the region beneath the mirror coils, despite the rising mirror coil current. The reaction currents generated by this leaked plasma prevented the magnetic field line reconnection required for achieving a magnetically detached plasma (an FRC). As the pulse progressed, plasma continued to leak out until bias flux was dissipated along with the plasma current.

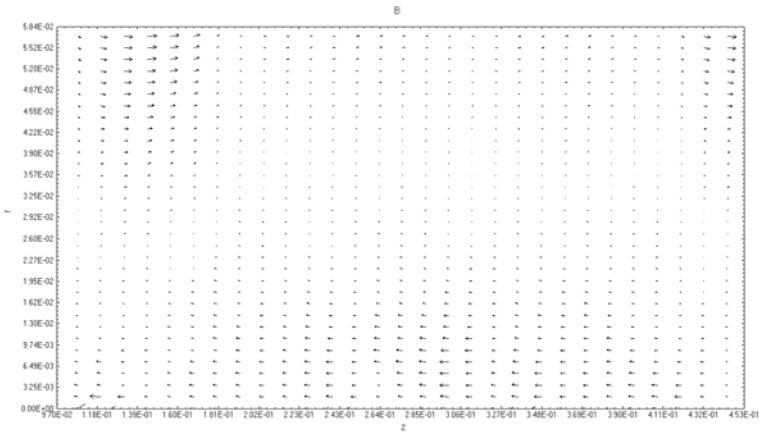

Figure 9: Magnetic field vector in r-z plane of the slug-target model showing field reversal with no reconnection.

This null result in the slug-preionization case was initially surprising, since many experiments that create FRCs use an effectively uniform preionization source. However, closer examination of the physical processes involved have revealed a limitation on the amount of plasma and magnetic flux that can be trapped in an FRC for a given set of field conditions.

If the plasma density or initial bias magnetic field are too high for the mirror field to confine during the implosion phase, then the plasma will leak out the ends until the excess density and trapped flux have dissipated enough to allow the field lines at the ends of the FRC to close. In the slug-case modeled above, this shedding of flux and density did not occur quickly enough and the plasma gradually collapsed without FRC formation. In order to force this closure, higher field strengths (more power) would be required.

D. Results Comparison

Of the three cases modeled, the annular helicon case produced the best FRC characteristics. In comparison to the conventional helicon preionization source, the annular helicon had more trapped flux and higher final mass. The higher trapped flux allows a greater force to be applied to the FRC and higher FRC mass provides higher thrust.

The uniform slug case did not form an FRC for the pulse conditions modeled, but these results were important because they demonstrate that there are limits on the amount of trapped flux and plasma that can be obtained for a given pulse field strength. The slug results also show that plasma leakage along the centerline of the system can prevent field reconnection, which is required for magnetic detachment and FRC formation. This suggests that there is an optimum bias field and total amount of plasma beyond which increased pulse power to the mirror coils is required to form the plasmoid. In addition, the presence of plasma on the centerline of the discharge seems to promote leakage; thereby preventing field line closure and FRC formation. Because the annular helicon minimizes the initial amount of on-axis plasma, this reconnection problem is minimized.

It is also important to note that the slug model assumed the same highly ionized plasma state as the annular model to allow comparison of the effects of using an annular plasma geometry rather than a slug. The local properties of the initial plasma (density and temperature) were held constant across these simulations. In a real system, using a conventional preionization technique, such as a DC discharge, to achieve the fully-ionized plasma conditions provided by a helicon discharge would be very difficult and less efficient. Thus the annular helicon preionization source has the combined benefits of high propellant ionization efficiency and good formation efficiency that are desired for space thruster applications.

IV. Experimental Investigation

The experimental investigation is designed to gain experience with pulse circuitry, pulse forming networks, and the diagnostics associated with these devices. The main goal is to produce an experiment that shows the development of the concept of the compact toroid propulsion system. This initial Phase I study is designed to simply test the fundamental principles of the physics of the device. Future Phase II experiments will use larger, higher-power hardware to fully simulate the annular helicon compact toroidal-plasma acceleration mechanism.

A. Apparatus and Setup

A pulse forming network is constructed to pulse current for plasma compression to gain experience with pulsed plasma diagnostics. The following sections describe the setup used to compress the plasma and the diagnostics being developed.

1. Pulse Forming Network

The pulse forming network (PFN) is designed based on the PFNs described by Glasoe and Lebacqz.[10] The PFN consists of a capacitor bank connected in series with a theta coil through a spark-gap switch. Initially, the capacitor bank is charged to the charging voltage, then the spark-gap is triggered and the stored charge is conducted through the circuit. The current conducted around the theta coil generates a strong magnetic field. This magnetic field is used to manipulate the plasma. A schematic representation of the PFN is shown in Figure 10.

2. Diagnostics

Diagnostics for measuring current, magnetic field, flux, and plasma properties were fabricated and used in the experimental investigation. A Rogowski coil was fabricated to measure the pulse current as a function of time. A Rogowski coil is a (typically) toroidal coil that samples a section of the time-varying magnetic flux due to a current passing through the axis of the toroid. The output voltage of the coil is proportional to the time derivative of the current according to the following equation, where $V_{Rogowski}$ is the Rogowski coil output, n is the number of turns, A is the area, I is the pulse current, and t is time.

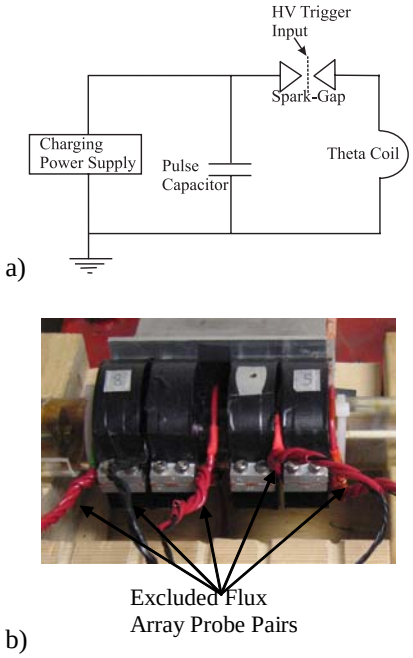

Figure 10: a) Schematic of the PFN and b) photograph of the theta coil with excluded flux array probe pairs.

$$V_{Rogowski} = \mu n A \frac{dI}{dt} \tag{2}$$

Magnetic field (B-dot) probes will also be utilized. These probes are typically a coil of wire that measures the time rate of change of a magnetic field through magnetic induction. These types of probes are used for the excluded flux array. The voltage output of the probe is proportional to the changing magnetic field through the following equation, where V_{Bdot} is the probe output voltage, and B is the magnetic flux density.

$$V_{Bdot} = nA \frac{dB}{dt} \tag{3}$$

An excluded flux array was also fabricated to measure the FRC excluded flux and separatrix radius. Excluded flux is the amount of magnetic flux excluded by the FRC, i.e. the flux that would be present inside the FRC separatrix if the FRC were not present. The separatrix radius is a measure of the physical size of the FRC. The excluded flux array consists of 5 probe pairs, where each pair consists of a flux loop and hair-pin loop magnetic field (B-dot) probe. Comparison of the magnetic field and flux during a vacuum shot (no plasma present) and a plasma shot with plasma present yields the excluded flux and separatrix radius according to the following equations, where ϕ_{exc} is the excluded flux, B_p is the magnetic flux density during a plasma shot, r_s is the separatrix radius, r_c is the theta coil radius, ϕ_p is the flux during a plasma shot, ϕ_v is the flux during a vacuum shot, and B_v is the magnetic flux density during a vacuum shot. Photographs of the excluded flux probes in the current experimental setup and the circuitry used to obtain real-time excluded flux measurements are shown in Figure 10.

$$\phi_{exc} = B_p \pi r_s^2 \tag{4}$$

$$r_s = r_c\left(1 - \frac{\phi_p}{\phi_v}\frac{B_v}{B_p}\right) \tag{5}$$

Also, a triple Langmuir probe was used to study the transient properties of the pulsed plasma. A triple Langmuir probe consists of three metal electrodes (typically cylindrical, refractory wires) that are placed in a plasma discharge to measure plasma properties such as electron density and temperature. This type of probe is ideal for the pulsed plasma experiment because it measures the electron temperature and density continuously. Unlike the traditional single Langmuir probe, voltage-sweeping is not required.[11] With the triple Langmuir probe, one of the electrodes is used to float the other two at the plasma floating potential. A floating power supply (typically batteries) provides a bias between two of the electrodes such that they enter the ion and electron saturation regimes. The potential difference between the floating electrode and electron saturation electrode is proportional to the electron temperature, while measurement of the ion saturation current yields the density. These types of probes have had extensive use in many other types of pulsed plasma devices.

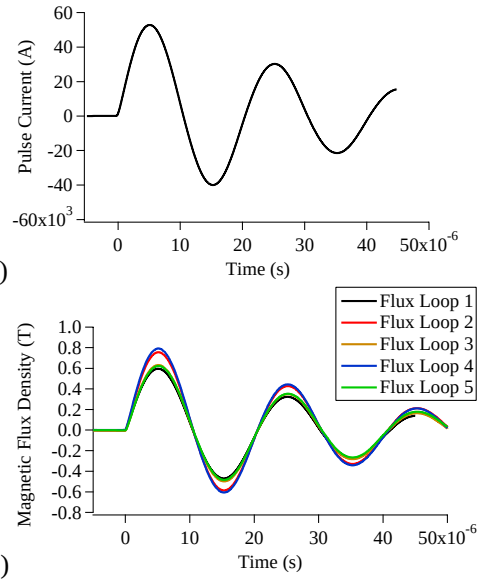

Figure 11: Experimental measurements of the a) pulse current waveform and b) magnetic flux density waveform for the 5 flux loops.

B. Experimental Results

Experimental results are presented in Figure 11, Figure 12, and Figure 13. An example current pulse waveform is shown in Figure 11. These data are for a capacitance of 94.6 μF and a charging voltage of 3.8 kV. The peak current is approximately 52 kA with a rise time (or quarter-wave time) of approximately 5 μs. The dI/dt associated with this waveform is sufficient enough to initiate breakdown of argon gas at 85 mTorr. That is, the current pulse generates a large azimuthal electric field that initiates breakdown of the argon gas and creates plasma during the pulse. This suggests that a preionization source may not be required; however, the resulting plasma may also be generated more slowly over several oscillations rather than the initial current rise. Full operation of the triple Langmuir probe is needed to distinguish the two possibilities. The magnetic flux density associated with the current pulse is measured by the five flux loops of the excluded flux array. Figure 11 shows the time evolution of the magnetic field for the five flux loops, while Figure 12 also shows the variation of the magnetic flux density as a function of spatial location along the theta coil. Notice that the peak magnetic flux density is approximately 0.8 T.

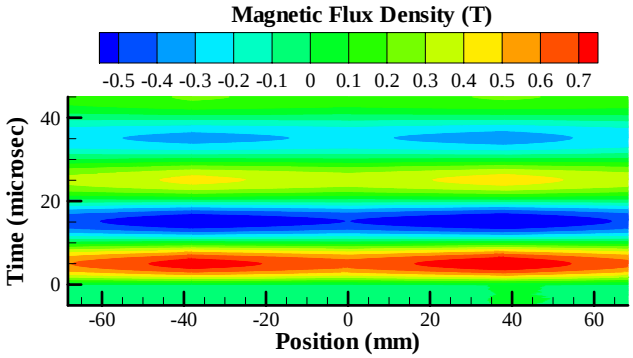

Figure 12: Experimental measurements of the time evolution of the magnetic field.

Figure 13 shows a photograph of the pre-pulse argon plasma along with a photograph taken during the current pulse. For this test, a preionized DC argon discharge is sustained by a power supply; auto-breakdown of the gas by the pulse is not used. This photograph was obtained by synchronizing the pulse discharge and a digital camera. Each photograph is a 1-second exposure of the plasma. Notice that the plasma color changes during the pulse. The initially pink, low-temperature argon plasma becomes more blue, which represents an increase in temperature. Furthermore, the increased temperature can be expected to give rise to a larger ionization fraction. These qualitative results are encouraging because they suggest that the magnetic field produced by the current pulse is affecting the plasma.

V. Conclusion

The use of an annular helicon preionization source for magnetically detached compact-toroid plasma accelerator offers the possibility of a high-efficiency, high-thrust variable specific-impulse thruster for OTV and other high-power/thrust applications. Early modeling efforts illustrate the benefits of the annular helicon source over its conventional counterpart due to increased trapped flux and larger area, thereby improving the coupling of the plasma to the pinch field and enabling FRC formation. Initial experiments to form and eject FRC plasmas are underway in parallel with diagnostic development.

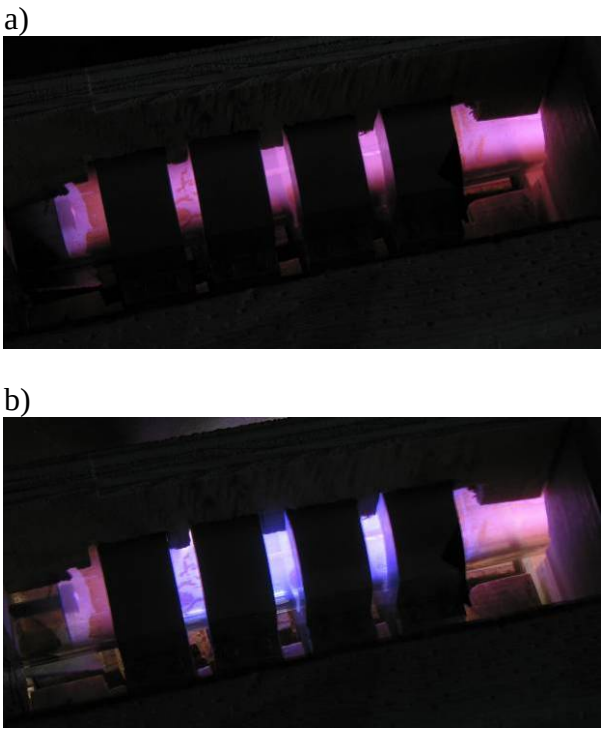

Figure 13: Photographs of the plasma discharge a) before and b) during a high-current (~57 kA) pulse. This shot is for a capacitance of 107 μF and charging voltage of 4.1 kV.

Acknowledgments

We would like to thank the entire research team at Starfire Industries and the High-Power Electric Propulsion Laboratory at Georgia Tech for being instrumental in this investigation. This research was sponsored by the Air Force Office of Scientific Research under a Phase I Small Business Technology Transfer award, contract number FA9550-06-C-0117, Mitat Birkan grant monitor.

References

[1]Taccetti, J. M., et al., "FRX-L: A field-reversed configuration plasma injector for magnetized target fusion," *Review of Scientific Instruments*, Vol. 74, No. 10, pp. 4314-4323, Oct. 2003.

[2]Zhang, S. Y., et al., "Confinement analyses of the high-density field-reversed configuration plasma in the field-reversed configuration experiment with a liner," *Physics of Plasmas*, Vol. 12, No. 5, May 2005.

[3]Yano, M., Williams, L., Walker, M. L. R., "Design and Operation of an Annular Helicon Plasma Source," *43rd Joint Propulsion Conference*, Cincinnati, OH., July 8-11, 2007.

[4]Cohen, S. A., Glasser, A. H., "Ion Heating in the Field-Reversed Configuration by Rotating Magnetic Fields near the Ion-Cyclotron Resonance," *Physical Review Letters*, Vol. 85, No. 24, pp. 5114-5117, Dec. 2000.

[5]Himura, H., et al., "Observation of collisionless thermalization of a plasmoid with a field-reversed configuration in a magnetic mirror," *Physics of Plasmas*, Vol. 5, No. 12, pp. 4262-4270, Dec. 1998.

[6]Slough, J. T., Hoffman, A. L., "Acceleration of a Field-Reversed Configuration for Central Fueling of ITER," *16th IAEA Fusion Energy Conference*, Montreal, Canada, Oct. 7-11, 1996.

[7]Rej, D. J., Tuszewski, M., "A zero-dimensional transport model for field-reversed configurations," *Physics of Fluids*, Vol. 27, No. 6, pp. 1514-1520, June 1984.

[8]Goldenbaum, G. C., Irby, J. H., Chong, Y. P., Hart, G. W., "Formation of a Spheromak Plasma Configuration," *Physical Review Letters*, Vol. 44, No. 6, pp. 393-396, Feb. 1980.

[9]Bellan, P. M., *Spheromaks: A Practical Application of Magnetohydrodynamic Dynamos and Plasma Self-Organization*, Imperial College Press, London, 2000.

[10]Glasoe, G. N., Lebacqz, J. V., *Pulse Generators*, MIT Radiation Laboratory Series, Vol. 5, L. N. Ridenour, ed., McGraw-Hill Book Company, Inc., New York, 1948.

[11]Chen, S.-L., Sekiguchi, T., "Instantaneous Direct-Display System of Plasma Parameters by Means of Triple Probe," *Journal of Applied Physics*, Vol. 36, No. 8, pp. 2363-2375, Aug. 1965.